

This is the Author's Pre-print version of the following article: *P. Álvarez-Alonso, C.O. Aguilar-Ortiz, E. Villa, A. Nespoli, H. Flores-Zúñiga, V.A. Chernenko, Conventional and inverse elastocaloric effect in Ni-Fe-Ga and Ni-Mn-Sn ribbons, Scripta Materialia, Volume 128, 2017, Pages 36-40*, which has been published in final form at <https://doi.org/10.1016/j.scriptamat.2016.09.033> This article may be used for non-commercial purposes in accordance with Terms and Conditions for Self-Archiving

Conventional and inverse elastocaloric effect in Ni-Fe-Ga and Ni-Mn-Sn ribbons

P. Álvarez-Alonso,^{1,a)} C.O. Aguilar-Ortiz,² E. Villa,³ A. Nespoli,³ H. Flores-Zúñiga,² and V.A. Chernenko^{4,5}

¹*Departamento de Electricidad y Electrónica, Universidad del País Vasco (UPV/EHU), 48940 Leioa, Spain*

²*División de Materiales Avanzados, IPICYT, 78216 San Luis Potosí, Mexico*


³*CNR IENI Unità di Lecco, 23900 Lecco, Italy*

⁴*Ikerbasque, Basque Foundation for Science, 48013 Bilbao, Spain*

⁵*BCMaterials & University of Basque Country (UPV/EHU), 48080 Bilbao, Spain*

Abstract

Magnetic shape memory $\text{Ni}_{55}\text{Fe}_{16}\text{Ga}_{29}$ and $\text{Ni}_{50}\text{Mn}_{40}\text{Sn}_{10}$ melt spun ribbons have been characterized by thermomechanical, mechanical, and dynamic-mechanical analysis. The martensitic transformation temperatures show an abnormal tendency to decline at a low stress range followed by a conventional increase above a threshold stress related to the internal compressive stress in the ribbon generated during the fabrication process. By studying the elastocaloric effect (eCE), an unusual behavior in shape memory alloys has been found: the ribbons present positive values of the entropy change induced by the tensile applied stress. This behavior results from shrinkage of the samples (instead of elongation) during the forward martensitic transformation under internal compressive stress giving rise to the caloric effect that can be termed as an inverse eCE. A contribution of the conventional eCE in the behavior of the total eCE is observed when applied stress overcomes the internal one. The conventional and inverse eCEs are attributed to the stress-induced forward and reverse martensitic transformation, respectively.

Solid state refrigeration represents a promising alternative to the gas compression/expansion refrigerant technology. It is based on the isothermal entropy (ΔS_{iso})/adiabatic temperature (ΔT_{ad}) changes in the caloric materials that are produced by the application of the external forces, such as, e.g., magnetic field or uniaxial stress.  The corresponding effects are called magnetocaloric (MCE) and elastocaloric

(eCE). Whereas MCE has been under intense studies over the past two decades, including materials exhibiting martensitic transformation (MT),² the research of eCE is still in its infancy. The first observation of eCE was done in a steel wire exhibiting a temperature increment of 0.16K at a tensile stress of 200MPa.³ A large reduction of temperature, about 3K, associated to the first-order antiferro-to-ferromagnetic phase transition induced by a tensile stress of 238MPa was observed in Fe-Rh.⁴ Then, the shape memory alloys (SMAs) have been put in the spotlight as they can experience large eCE associated to the thermomechanically driven MT.⁵ For instance, ΔT_{ad} equal to 25.5K (at stress of 650MPa), 9K (400MPa), and 14.2K (500MPa) has been obtained in wires, thin films, and single crystals of NiTi, respectively,⁶⁻⁸ while 6K (275MPa) in bulk Cu-Zn-Al.⁹ A considerable eCE has been observed also in the bulk magnetic SMAs, such as Ni-Mn-In-Co (3.5K at 100MPa),¹⁰ Ni-Mn-Ga-Fe ($\Delta S_{iso} = -5.5\text{J/kgK}$ at 9.3MPa),¹¹ Ni-Mn-Sb-Co ($\Delta S_{iso} = -20\text{J/kgK}$ at 104MPa),¹² and Ni-Mn-Sn ($\Delta S_{iso} = -1.7\text{J/kgK}$ at 5.2 MPa,¹³ $\Delta T_{ad} = -5.7\text{K}$ at 242MPa¹⁴), as well as Ni-Fe-Ga single crystal ($\Delta T_{ad} = 8.4\text{K}$ at 50MPa) and polycrystalline ($\Delta T_{ad} = 6\text{K}$ at 133MPa).^{8,15}

Taking into account that mentioned entropy and temperature changes mechanically driven are much easier and less expensive to obtain than magnetically, together with the wide temperature window and diversity in the applied stress modes (tensile, compressive, bending or twist stresses), the mechanical refrigeration deserves reinforced research efforts.¹⁶ In this letter, we present the thermomechanical behavior and deduced conventional and abnormal eCE responses of two ribbons of Ni-Fe-Ga (R1) and Ni-Mn-Sn (R2) SMAs affected by the internal stress. The ribbon geometry ensures a reduced thermal inertia whereby allowing increasing cycling frequencies and cooling power of refrigerant systems, which are important for applications.¹⁷

Details of the fabrication of as-quenched $\text{Ni}_{55}\text{Fe}_{16}\text{Ga}_{29}$ and $\text{Ni}_{50}\text{Mn}_{40}\text{Sn}_{10}$ ribbons and their differential scanning calorimetry (DSC) measurements can be found elsewhere.¹⁸ Microstructure and composition were probed by scanning electron microscopy (SEM) using a FEI/Philips XL30 FEG ESEM equipped with an energy dispersive spectroscopy (EDS) system. X-ray diffraction (XRD) patterns were collected with a Bruker AXS model D8 Advance diffractometer using $\text{Cu-K}\alpha$ radiation. The mechanical tests were performed in a Q800 TA Instruments Dynamic Mechanical Analyzer (DMA) using both the dynamic

mode (temperature rate of 2K/min, strain amplitude of 10^{-4} and frequency of 1Hz) and static one. In a static mode, the temperature dependences of strain, $\varepsilon(T)$, under constant load applied along the ribbons axis were registered with temperature rate of 5K/min. Furthermore, isothermal stress-strain, σ - ε , curves were measured in a stress control mode starting from high temperatures with a maximum load set at 200 and 100MPa for R1 and R2, respectively, to avoid sample failure.

Previous DSC measurements of R1 and R2¹⁸ enabled the determination of characteristic MT temperatures, M_s , M_f , A_s , and A_f , average transformation enthalpy, ΔH , and corresponding value of transformation entropy, $\Delta S = \Delta H/T_0$, where $T_0 = (M_s + A_f)/2$, which are shown in Table I. Thermal hysteresis of MT (defined as $\Delta T = A_f - M_s$) reflects its first-order character. Note the reduced value of $\Delta T \approx 8\text{K}$ for R2, which has been also observed in similar Ni-Mn-Sn-Fe ribbons.¹⁹

Figure 1 depicts the room temperature XRD patterns of both ribbons. No clear crystallographic texture is observed. The peaks belong to a martensite phase having 14M monoclinic structure (space group P2/m) with cell parameters $a = 4.331\text{\AA}$, $b = 2.687\text{\AA}$, $c = 29.143\text{\AA}$, and $\beta = 93.0^\circ$ for R1, and 6M orthorhombic structure (space group P222) with cell parameters $a = 36.42\text{\AA}$, $b = 5.93\text{\AA}$ and $c = 5.59\text{\AA}$ for R2. No secondary phases are observed. Insets in Fig. 1 present the SEM microstructures of the ribbons free-faces. The ribbons exhibit a broad grain size distribution enhancing their brittleness. In ribbon R1, the grains consist of a number of the bubble-like features. In this case, grain boundaries, one of those is highlighted in the inset in Fig. 1(a), can be hardly traced by the same oriented packets of martensitic twins since adjacent grains can also serve as a continuation to the same oriented martensitic microstructure. Ribbon R2 does not show the mentioned features and grain boundaries can be easily discerned (see inset in Fig. 1(b)).

The temperature variation of the elastic modulus in both ribbons in Fig. 2 presents hysteretic anomalies typical for MTs. The wider hysteresis in Fig. 2 than in the DSC curves shown in Ref. 18 is explained by an absence of direct thermal contact of thermocouple with the sample in DMA. Note the very low values of the elastic modulus in both phases and their large relative change across MT. The similar behavior occurs in other SMA ribbons although to a less extent (see, e.g., Ref. 20).

Figures 3(a, b) depict the $\varepsilon(T)$ curves measured under constant tensile loads. The observed length contraction with increasing temperature (outside the temperature range of MT) is related to a change of the offsets between the temperatures and thermal expansions of the sample and its holder, which cannot be removed due to the instrumental limitations of the DMA machine not designed for such measurements. The observed negative slopes of the thermal expansion in the martensitic and austenitic phases have a negligible contribution to the calculated entropy change and/or selection of the transformation temperatures as only the steep deformation process produced by MT was counted.

Curves in Figs. 3(a, b) demonstrate a unique tensile stress dependence of the transformation-induced strain in the ribbons from a contraction, instead of elongation, during the forward MT at low values of stress to the expected expansion at high external stress. Similar behavior was observed in the bulk Ni-Ti SMA heat-treated under constraint conditions.^{21,22} The process of the change of sign of transformation strain is also accompanied by the appearance of a “loops-like” anomalous character of the full $\varepsilon(T)$ curves such as for R2 at 25MPa, as the most pronounced case. The expected regular $\varepsilon(T)$ behavior for R2 was impossible to record since higher values of stress always caused a sample failure. According to Figs. 3(a, b), the reversible strain anomaly disappears at some threshold value of the applied stress situated between 5 and 10MPa for R1 and between 15 and 20MPa for R2. It is reasonable to attribute these stresses to the internal compressive stress, σ^{int} , in the ribbons, which opposes the tensile applied load, because an unstressed martensite presents a negligible deformation due to the self-accommodated substructure. Such a situation was not found in the other shape memory ribbons such as Ni-Mn-Ga or NiTi.²³ One of the reasons could be the obviously positive value of the internal stress in those cases.²⁴ We suggest that the measurements shown in Figs. 3(a, b) and their treatment below, allow to quantify σ^{int} . The melt-spinning fabrication procedure results in the defect structure of SMAs ribbons, which influences their thermodynamic properties through the mechanism of internal stress effects.²⁵ In the case of bulk Ni-Ti, the internal stress was created by the coherent precipitates.^{21,22} Figures 3(c, e) evidence that an existence of σ^{int} also leads to the abnormal behavior of the phase diagram ‘transformation temperatures versus stress’, which is manifested by the negative slopes at small stresses, especially in the case of R2. This provide a possibility of stress-induced reverse MT, which was observed in the bulk Ni-Ti^{21,22} and Ni-Mn-

Ga²⁶ alloys, where the internal stress was created by the precipitates in the former and application magnetic field in the latter. Above some threshold stress, which corresponds to the σ^{int} , the phase diagrams show a conventional behavior with the positive slopes. In terms of $T_0(\sigma)$, these slopes are equal to $dT_0/d\sigma \approx 0.17$ and $\approx 0.52\text{K/MPa}$ for R1 and R2, respectively. Incidentally, both negative and positive slopes are in a qualitative agreement with a Clausius-Clapeyron relationship, $dT_0/d\sigma = \Delta S/\varepsilon_{\text{tr}}$ (ε_{tr} is transformation strain), bearing in mind that in the negative case σ and ε_{tr} have opposite signs. This situation is reminiscent to the magnetic case,²⁷ where the part of ' T_0 versus field' phase diagram with negative slope is explained by a dominant role of the magnetocrystalline anisotropy. For the mechanical analog of present work, an internal stress should play the same role.

The enhanced brittleness of the ribbons prevented obtaining close loops of superelastic curves above A_f temperature since higher stress levels, needed for that, caused samples failure. Selected σ - ε curves measured in austenite, just above M_s , are depicted in Figs. 3(d, f). They demonstrate a stress-induced forward MT in a drastically different manner. Whereas R1 shows a partial superelastic recovery, typical for other SMAs, R2 exhibits entirely abnormal behavior. In the latter case, Fig. 3(d) shows that the strain evolution is linear from a to b in austenite with a very low slope due to small elastic modulus (see Fig. 2), then the ribbon shrinks, $b - c$, instead of elongation, reflecting influence of σ^{int} on the tensile stress-induced MT. Once σ^{int} of around 20MPa is overtaken, point c , the sample is in the martensite phase and presents a normal linear behavior, $c-d-e$, with a much higher elastic modulus (cf. Fig. 2 and Fig. 3(b)). This behavior is reproducible after resetting the sample by heating into the austenite, Fig. 3(f).

The sources of eCE can be a remarkable variation of the Young's modulus with the temperature,²⁸ and a thermomechanically induced first-order phase transformation,¹¹ both accompanied by large changes in the temperature dependence of the strain. Based on $\varepsilon(T)$ data in Figs. 3(a, b), the temperature dependences of the stress-induced entropy have been calculated by a Maxwell relationship:²⁷ $\Delta S_{\text{iso}}(T, \sigma) = \int_0^\sigma \frac{\partial \varepsilon(T, \sigma)}{\partial T} d\sigma$

Figure 4(a) shows that ribbons exhibit both the conventional (negative entropy change) and inverse (positive entropy change) eCE in the reverse proportions. Figure 4(a) and the stress dependences of entropy change maxima in Fig. 4(b) reveal that R1 below $\sim 10\text{MPa}$ presents a tiny inverse eCE being replaced by the appearance and fast increase of the conventional eCE above this stress value. The latter

eCE is commonly observed in the materials undergoing a stress-induced forward MT.¹¹ On the other hand, R2 exhibits a very pronounced inverse eCE, unusual for SMAs, which starts to decrease around 17MPa due to increasing contribution of conventional eCE that dominates up to the stress limit achieved. Extrapolation shown in Fig. 4(b) assumes a disappearance of inverse eCE in R2 at about 30MPa. In terms of the results shown in Fig. 4(b), the value of internal stress should correspond to the maximum on the curve $\Delta S_{\text{iso}}^{\text{peak}}$ versus stress. Taking into account the error bars, one may consider -7 ± 2 and -17 ± 3 MPa as the acceptable approximations of σ^{int} for R1 and R2, respectively.

So far, a phenomenon of the inverse eCE was reported in Fe-Rh alloy as a result of the specific volume contraction accompanying the tensile-stress-induced isostructural transition.^{4,29} In the case of SMA ribbons studied in the present work, the inverse eCE under tensile load appears as a result of the combined influence of the internal compressive and applied tensile stresses on MT. This phenomenon can be considered as a mechanical analog of the inverse MCE observed in Ni-Mn-Ga alloy below the anisotropy field.²⁹ Likewise the magnetic field-induced reverse MT is a source of the inverse MCE in the metamagnetic SMAs,²⁹ the negative slope of T_0 versus external stress in the phase diagrams, such as shown in Fig. 3(e), means that the inverse eCE observed in the present work should be attributed to the stress-induced reverse MT.

In summary, the thermomechanical measurements of the Ni-Fe-Ga and Ni-Mn-Sn ribbons revealed their abnormal behaviors at low tensile stress, such as a decrease in both the MT temperature and the transformation-induced strain, giving rise to a phenomenon of inverse eCE. These behaviors start to compete with the conventional ones above some threshold value of the applied stress, which is interpreted as the manifestation of an internal stress of opposite sign formed in the material during quenching from liquid state. These results and approaches have didactic importance as well as they can be interesting for practical use.

Financial support from projects No. CB-2010-01-157541 (CONACYT, Mexico), MAT2014-56116-C4-3-4-R (Spanish Ministry of Economy and Competitiveness), and Laboratorio Nacional de

Investigaciones en Nanociencias y Nanotecnología (LINAN,IPICyT) is acknowledged. Technical support provided by Beatriz Adriana Rivera Escoto is gratefully acknowledged.

References

- ¹ S. Crossley, N.D. Mathur, and X. Moya, *AIP Adv.* **5**, 67153 (2015).
- ² J. Liu, T. Gottschall, K.P. Skokov, J.D. Moore, and O. Gutfleisch, *Nat. Mater.* **11**, 620 (2012).
- ³ V.V. Sychev, *Complex Thermodynamic Systems* (Springer Science & Business Media, 2013).
- ⁴ S.A. Nikitin, G. Myalikgulyev, M.P. Annaorazov, A.L. Tyurin, R.W. Myndyev, and S.A. Akopyan, *Phys. Lett. A* **171**, 234 (1992).
- ⁵ E. Bonnot, R. Romero, L. Mañosa, E. Vives, and A. Planes, *Phys. Rev. Lett.* **100**, (2008).
- ⁶ J. Cui, Y. Wu, J. Muehlbauer, Y. Hwang, R. Radermacher, S. Fackler, M. Wuttig, and I. Takeuchi, *Appl. Phys. Lett.* **101**, 73904 (2012).
- ⁷ C. Bechtold, C. Chluba, R.L. de Miranda, and E. Quandt, *Appl. Phys. Lett.* **101**, 91903 (2012).
- ⁸ G.J. Pataky, E. Ertekin, and H. Sehitoglu, *Acta Mater.* **96**, 420 (2015).
- ⁹ L. Mañosa, S. Jarque-Farnos, E. Vives, and A. Planes, *Appl. Phys. Lett.* **103**, 211904 (2013).
- ¹⁰ B. Lu, F. Xiao, A. Yan, and J. Liu, *Appl. Phys. Lett.* **105**, 161905 (2014).
- ¹¹ D.E. Soto-Parra, E. Vives, D. González-Alonso, L. Mañosa, A. Planes, R. Romero, J.A. Matutes-Aquino, R.A. Ochoa-Gamboa, and H. Flores-Zúñiga, *Appl. Phys. Lett.* **96**, 71912 (2010).
- ¹² R. Millán-Solsona, E. Stern-Taulats, E. Vives, A. Planes, J. Sharma, A.K. Nayak, K.G. Suresh, and L. Mañosa, *Appl. Phys. Lett.* **105**, 241901 (2014).
- ¹³ P.O. Castillo-Villa, L. Mañosa, A. Planes, D.E. Soto-Parra, J.L. Sánchez-Llamazares, H. Flores-Zúñiga, and C. Frontera, *J. Appl. Phys.* **113**, 53506 (2013).
- ¹⁴ W. Sun, J. Liu, B. Lu, Y. Li, and A. Yan, *Scr. Mater.* **114**, 1 (2016).
- ¹⁵ Y. Xu, B. Lu, W. Sun, A. Yan, and J. Liu, *Appl. Phys. Lett.* **106**, 201903 (2015).

- ¹⁶ B. Lu and J. Liu, *Sci. Bull.* **60**, 1638 (2015).
- ¹⁷ S. Qian, J. Ling, Y. Hwang, R. Radermacher, and I. Takeuchi, *Int. J. Refrig.* **56**, 65 (2015).
- ¹⁸ E. Villa, C.O. Agilar-Ortiz, P. Álvarez-Alonso, J.P. Camarillo, G.A. Lara-Rodriguez, H. Flores-Zúñiga, and V.A. Chernenko, *MATEC Web Conf.* **33**, 5009 (2015).
- ¹⁹ C.O. Aguilar-Ortiz, D. Soto-Parra, P. Álvarez-Alonso, P. Lázpita, D. Salazar, P.O. Castillo-Villa, H. Flores-Zúñiga, and V.A. Chernenko, *Acta Mater.* **107**, 9 (2016).
- ²⁰ V.A. Chernenko, B.R. Kanth, P.K. Mukhopadhyay, S.N. Kaul, E. Villa, A. Gambardella, and S. Besseghini, *Appl. Phys. Lett.* **93**, 141904 (2008).
- ²¹ T. Fukuda, A. Deguchi, T. Kakeshita, and T. Saburi, *Mater. Trans. JIM* **38**, 514 (1997).
- ²² T. Fukuda, M. Takahata, T. Kakeshita, and T. Saburi, *Mater. Trans.* **42**, 323 (2001).
- ²³ J. Pons, E. Cesari, R. Santamarta, and V.A. Chernenko, *Advances in Mechanical Behaviour, Plasticity and Damage* (Elsevier, 2000).
- ²⁴ E.L. Cuellar, E.N. Mendoza, C.J.D. Araújo, B.C.L. Walle, J. Otubo, and C. Gonzalez, *Mater. Res.* (2016). On-line version.
- ²⁵ V.A. Chernenko, V.V. Kokorin, and I.N. Vitenko, *Smart Mater. Struct.* **3**, 80 (1994).
- ²⁶ H. E. Karaca, B. Basaran, I. Karaman, and Y.I. Chumlyakov, *Smart Mater. Struct.* **21**, 045011 (2012).
- ²⁷ T. Fukuda, H. Maeda, M. Yasui, and T. Kakeshita, *Scr. Mater.* **60**, 261 (2009).
- ²⁸ F. Xiao, T. Fukuda, and T. Kakeshita, *Appl. Phys. Lett.* **102**, 161914 (2013).
- ²⁹ L. Mañosa, A. Planes, and M. Acet, *J. Mater. Chem. A* **1**, 4925 (2013).

Figure captions

Figure 1: XRD patterns for Ni-Fe-Ga (a) and Ni-Mn-Sn (b) ribbons. Insets: SEM images of the ribbons free surfaces. Dash line traces one of the grains in R1 ribbon.

Figure 2: Temperature dependence of the elastic modulus for the studied ribbons. The measuring tensile strain amplitude is 0.02% for Ni-Fe-Ga and 0.03% for Ni-Mn-Sn.

Figure 3: Temperature dependences of strain, $\varepsilon(T)$, under constant tensile loads applied at high temperatures in accumulative manner with the step of 5MPa (a, b); characteristic temperatures of MT (obtained by tangent method from $\varepsilon(T)$ dependences) as a function of the applied stress (c, e); and selected stress-strain curves (d, f) for Ni-Fe-Ga and Ni-Mn-Sn ribbons. The critical transformation stresses are indicated in (d) by horizontal dash lines.

Figure 4. Temperature dependences of isothermal entropy changes (a) and their peak values (b) under different applied stress for Ni-Fe-Ga and Ni-Mn-Sn ribbons. Dotted curves are the extrapolations to higher stresses.

Table 1: Characteristic temperatures, average transformation enthalpy, ΔH , and entropy, ΔS , as well as thermal hysteresis, ΔT , of the martensitic transformation exhibited by R1 and R2 ribbons.

Ribbon	Composition (at. %)	M_s (K)	M_f (K)	A_s (K)	A_f (K)	ΔH (J/g)	ΔS (J/kgK)	ΔT (K)
R1	Ni _{55.1} Fe _{16.2} Ga _{28.7}	359	337	350	371	4.6	12.7	12.0
R2	Ni _{50.3} Mn _{39.7} Sn _{10.0}	427	416	430	435	23.1	53.5	8.0